

Effect of Drying Time on Electrochemical Properties of $\text{Li}_{1.2}\text{Mn}_{0.54}\text{Ni}_{0.13}\text{Co}_{0.13}\text{O}_2$ Cathode Material

Changkun Song², Wangjun Feng^{1,2,*}, Wenxiao Su², Linjing Chen², Miaomiao Li²,

¹ State Key Laboratory of Advanced Processing and Recycling Nonferrous Metals, Lanzhou University of Technology, Lanzhou 730050, China;

² School of Science, Lanzhou University of Technology, Lanzhou 730050, China

*E-mail: wjfeng@lut.cn

Received: 7 October 2018 / Accepted: 29 November 2018 / Published: 7 February 2019

Li-rich layered cathode materials were synthesized by the sol-gel method with acetate and citric acid. The effect of drying time on the structure, morphology and electrochemical properties of the prepared material were carefully studied with X-ray diffraction (XRD), scanning electron microscopy (SEM), cyclic voltammetry (CV), electrochemical impedance spectroscopy (EIS) and electrochemical characterization. The results show that the $\text{Li}_{1.2}\text{Mn}_{0.54}\text{Ni}_{0.13}\text{Co}_{0.13}\text{O}_2$ sample had a uniform particle size distribution and outstanding electrochemical performance at 24 h drying time. It delivered the largest initial discharge capacity of 262.5 mAh/g and coulombic efficiency of 77.66% at 0.1 C. Furthermore, it showed a high discharge capacity of 200.1 mAh/g and 158.9 mAh/g at 0.5 C and 2 C and a capacity retention of 80.46% and 84.14% after 100 cycles, respectively.

Keywords: Li-rich; Lithium-ion batteries; drying time; capacity retention

1. INTRODUCTION

In recent years, with the continuous development of electrochemical energy storage technology, rechargeable batteries have received worldwide attention. Lithium-ion batteries are widely used in portable storage devices due to their high energy density and environmental friendliness [1-4]. However, conventional cathode materials, such as layered LiCoO_2 , $\text{Li}[\text{Mn}_{1/3}\text{Ni}_{1/3}\text{Co}_{1/3}]\text{O}_2$, spinel type LiMn_2O_4 and olivine type LiFePO_4 , are unable to meet the requirements of higher capacity and higher energy density required for practical applications [5,6]. Hence, it is a major challenge to explore the new generation of high-capacity cathode materials [7].

Lithium-rich layered oxide is a relatively new cathode material for lithium ion batteries, which can be expressed by the general formula $x\text{Li}_2\text{MnO}_3(1-x)\text{LiMO}_2$ (M=Ni, Co, Mn). The reversible

specific capacity reaches 230-285 mAh/g, which has been widely studied for practical applications [8,9]. Among these materials, $\text{Li}_{1.2}\text{Mn}_{0.54}\text{Ni}_{0.13}\text{Co}_{0.13}\text{O}_2$ has a theoretical specific capacity of 377 mAh/g. It has high initial coulombic efficiency and excellent rate performance [10]. According to the study, $\text{Li}_{1.2}\text{Mn}_{0.54}\text{Ni}_{0.13}\text{Co}_{0.13}\text{O}_2$ can also be rewritten as $0.5\text{Li}_2\text{MnO}_3 \cdot 0.5\text{LiNi}_{1/3}\text{Co}_{1/3}\text{Mn}_{1/3}\text{O}$ with two-component notation, which can provide an initial discharge capacity of up to 250 mAh/g between 2.0 and 4.8 V at room temperature [11].

Generally, the electrochemical properties of prepared electrode materials are affected by purity, phase crystallinity, particle size and distribution. These influencing factors are mainly determined by the preparation methods [12]. At present, researchers mainly use the sol-gel method [4], solid phase method [13,14], coprecipitation method [15], hydrothermal method [16] and other synthetic methods to prepare lithium-rich layered materials. The sol-gel method is highly preferred for the synthesis of LLMO by combining with transition metal ions at sub-atomic levels of the starting sol to synthesize uniform, stoichiometric nanoparticles [8].

In this work, we first studied the morphology and electrochemical properties of $\text{Li}_{1.2}\text{Mn}_{0.54}\text{Ni}_{0.13}\text{Co}_{0.13}\text{O}_2$ by varying the drying time of the gel, namely at 12 h, 24 h and 36 h. The results show that the morphology of the material is optimal and has the best performance when the drying time is 24 h. The initial discharge specific capacity at the optimal condition is as high as 262.5 mAh/g, which is much higher than the other two drying times, whose first discharge specific capacity at 0.5 C and 2 C reaches 200.1 mAh/g and 158.9 mAh/g, respectively. The capacity at 0.5 C and 2 C remains at 161.0 mAh/g and 133.7 mAh/g after 100 cycles, respectively.

2. EXPERIMENTAL PROCEDURE

2.1. Material preparation

In this experiment, the $\text{Mn}(\text{CH}_3\text{COO})_2 \cdot 4\text{H}_2\text{O}$, $\text{Ni}(\text{CH}_3\text{COO})_2 \cdot 4\text{H}_2\text{O}$, and $\text{Co}(\text{CH}_3\text{COO})_2 \cdot 4\text{H}_2\text{O}$ molar ratios of 54:13:13 were first dissolved in a certain amount of deionized water and recorded as a TM solution. $\text{CH}_3\text{COOLi} \cdot 2\text{H}_2\text{O}$ and $\text{C}_6\text{H}_8\text{O}_7 \cdot \text{H}_2\text{O}$ were then dissolved in deionized water at a molar ratio of 6:5 to form a solution. Finally, the TM solution was slowly dropped into the above solution and continuously stirred, followed by the addition of aqueous ammonia to adjust the pH of the solution to 9 to form the final mixed solution. Next, the mixed solution was placed in a water bath as a sol-gel at 80 °C, and when it was stirred to a gel-like substance, it was placed in a drying oven at 140 °C for 12 h, 24 h and 36 h to obtain different samples. The obtained sample was ground, placed in a tube furnace, pre-fired at 450 °C for 8 hours in the air, and then removed and ground again. Then, it was further placed in a tube furnace and sintered at a high temperature of 850 °C for 8 hours to obtain the precursor. The synthesis process is illustrated in Fig. 1.

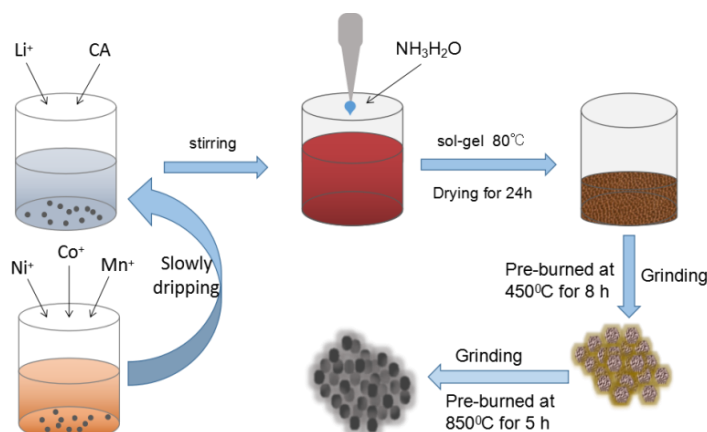


Figure 1. Schematic diagram of the formation process of materials.

2.2 Material characterization

X-ray diffraction (XRD) measurements were performed using a Bruker D8 Advance diffractometer with Cu K α radiation. The range of diffraction data collection was $10^\circ < 2\theta < 80^\circ$. The morphological characteristics of the samples were observed using a JSM-6700F scanning electron microscope (SEM), and the accelerating voltage was 20 KV. The TEM (JEM-2100F) images of the samples were collected at 200 KV.

2.3 Preparation of cathode and electrochemical analysis

The positive electrode of the battery consists of 80% $\text{Li}_{1.2}\text{Mn}_{0.54}\text{Ni}_{0.13}\text{Co}_{0.13}\text{O}_2$ composites, 10% acetylene black as the conductive material and 10% polyvinylidene fluoride (PVDF) as the binder by adding a certain amount of 1-methyl-2-pyrrolidone (NMP) as the solvent. The slurry was then uniformly applied to an aluminium foil and placed in a dry box. The battery assembly consisted of a positive electrode material and a lithium metal negative electrode separated by a Celgard 2400 polyethylene/polypropylene membrane. The electrolyte was made of 1 mol/L LiPF_6 dissolved in EC/DMC/DEC (1:1:1 by volume). The battery was assembled in a sealed argon-filled glove box. The charge and discharge test of the battery was carried out using the LAND-CT2001A Battery Test System (Wuhan, China) between 2.0 V and 4.8 V at room temperature. Electrochemical impedance spectroscopy (EIS) and cyclic voltammetry (CV) studies were performed at electrochemical workstations. The EIS was recorded in the frequency range of 10^{-2} Hz to 10^5 Hz when the potential difference signal amplitude was 5 mV. The CV test voltage range was 2.0-4.8 V, and the scan rate was 0.1 mV/s.

3. RESULTS AND DISCUSSION

3.1. Crystalline structure analysis

The crystal structure of the sample was determined by XRD analysis. Fig. 2 shows the XRD

spectra of the $\text{Li}_{1.2}\text{Mn}_{0.54}\text{Ni}_{0.13}\text{Co}_{0.13}\text{O}_2$ material at different drying times. The spectra do not contain any impurity phases, and the diffraction peaks are sharp and strong, indicating a high crystallinity and pure phase content. The apparent splitting of the (006)/(102) and (108)/(110) peaks in the XRD spectrum indicates that the material had a well-organized layered structure [17,18]. The peak splitting of the dried 24 h sample in Fig. 2 is most pronounced, so the corresponding material had the best layered structure.

The lattice parameters a and c are related to the average metal-metal intra-slab and inter-slab distance, respectively. A crystalline layer structure formed when the c/a values of all samples were larger than 4.899. [6] The ratio of $I(003)/I(104)$ in the XRD pattern is an important factor in the degree of cation mixing in the material; when $I(003)/I(104) < 1.2$, the degree of cation mixing in the material is high. If the ratio of $I(003)/I(104)$ is larger, the degree of cation mixing is low [19-21]. By calculating the $I(003)/I(104)$ values at different drying times (Table 1), we found that $I(003)/I(104) > 1.2$, and the $I(003)/I(104)$ value is the largest when the drying time was 24 h. Therefore, when the drying time is 24 h, the cation mixing degree is the lowest and the electrochemical performance is optimal.

Table 1. Lattice parameters of the different drying time samples.

Samples	$a(\text{\AA})$	$c(\text{\AA})$	c/a	$I(003)/I(104)$
12 h	2.8469	14.2371	5.00	1.06
24 h	2.8502	14.2310	4.99	1.38
36 h	2.8499	14.2323	4.99	1.16

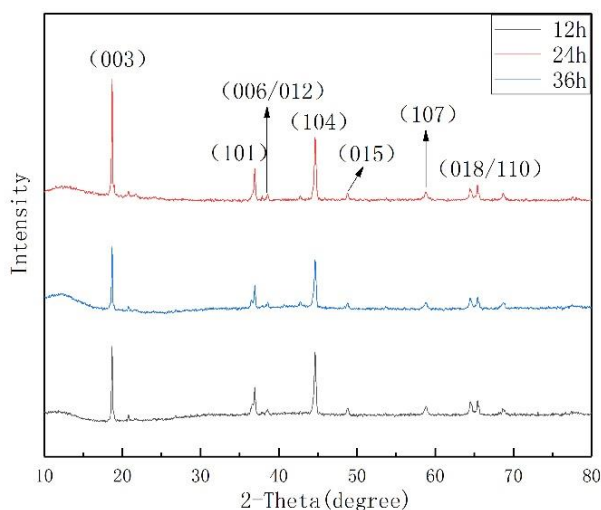


Figure 2. XRD patterns of various $\text{Li}_{1.2}\text{Mn}_{0.54}\text{Ni}_{0.13}\text{Co}_{0.13}\text{O}_2$ at different drying times.

3.2 Morphological observation

The morphology and particle size of the electrode material had a large effect on the

electrochemical performance. Fig. 3 (a) and (b) shows SEM images of the $\text{Li}_{1.2}\text{Mn}_{0.54}\text{Ni}_{0.13}\text{Co}_{0.13}\text{O}_2$ material at a drying time of 24 h. The samples were all ellipsoidal, and the particle size was approximately uniform. The smaller the particle size of the material, the shorter the diffusion path of the lithium ions inside the material, which is beneficial for improving the shuttle of lithium ions in the material [17,22,23].

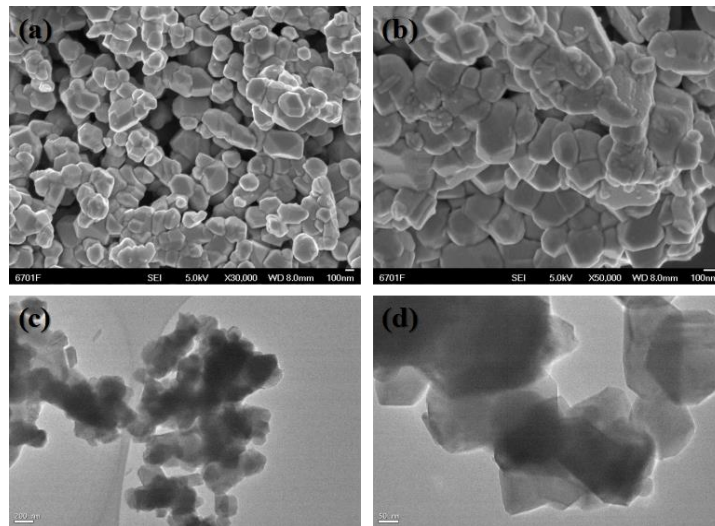


Figure 3. (a) and (b) SEM images of $\text{Li}_{1.2}\text{Mn}_{0.54}\text{Ni}_{0.13}\text{Co}_{0.13}\text{O}_2$; (c) and (d) TEM images of $\text{Li}_{1.2}\text{Mn}_{0.54}\text{Ni}_{0.13}\text{Co}_{0.13}\text{O}_2$.

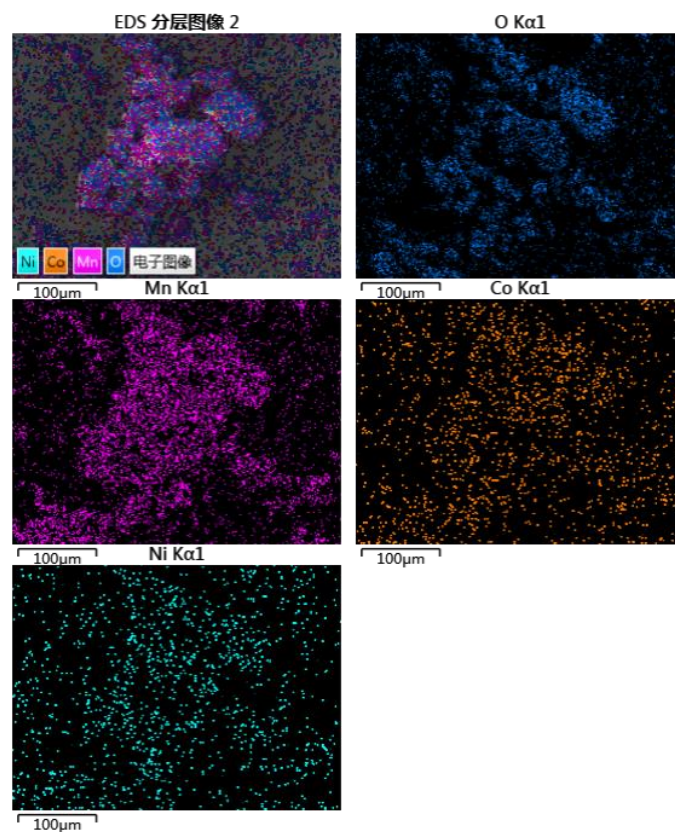


Figure 4. EDS mapping of Ni, Co and Mn based on the $\text{Li}_{1.2}\text{Mn}_{0.54}\text{Ni}_{0.13}\text{Co}_{0.13}\text{O}_2$ material at a drying time of 24 h.

The sample consisted of uniform particles with a size in the range of 100-300 nm. It had better electrochemical performance. Fig. 3 (c) and (d) shows TEM images of the $\text{Li}_{1.2}\text{Mn}_{0.54}\text{Ni}_{0.13}\text{Co}_{0.13}\text{O}_2$ material at a drying time of 24 h. Single-phase, well-surfaced octahedral crystallites are observed with sizes ranging from 100 nm to 400 nm. Fig. 4 is a schematic diagram of EDS mapping of $\text{Li}_{1.2}\text{Mn}_{0.54}\text{Ni}_{0.13}\text{Co}_{0.13}\text{O}_2$ particles based on the inset of Fig. 3. As shown in Fig. 4, the chemical was directly related to the strength of the element. Ni, Co and Mn were evenly and consistently distributed. The EDS element mapping image clearly shows that Ni, Co and Mn elements were uniformly distributed in the $\text{Li}_{1.2}\text{Mn}_{0.54}\text{Ni}_{0.13}\text{Co}_{0.13}\text{O}_2$ sample [8,24].

3.3 Electrochemical performance

Fig. 5 is the first charge and discharge curve of each sample at 0.1 C rate. The first charging process for the lithium-rich manganese-based solid solution materials can be divided into two steps: an S-shaped curve below 4.5 V and an L-shaped platform above 4.5 V. Below 4.5 V, lithium ions were removed from the LiMO_2 component of the material, and above 4.5 V, Li_2O was removed from the Li_2MnO_3 component [6,25]. Due to the appearance of the 4.5 V platform, a capacity that exceeds the redox calculation of the transition metal element in the layered material was produced. A specific capacity of more than 200 mAh/g was maintained in the next charge and discharge (2 to 4.8 V). As shown in Fig. 5, the three different drying times correspond to different first charge and discharge capacities. Among them, the charge-discharge specific capacity of drying for 24 hours was the highest, reaching 338.0 and 262.5 mAh/g, and the capacity retention rate was 77.66%. Compared with the positive electrode materials prepared by other methods, the positive electrode material obtained by this method had more attractive properties. (Table 2)

Table 2. Performance comparison of materials obtained by various methods

method	Molecular formula	Charge capacity (0.1 C)	Discharge capacity (0.1 C)	retention rate	Ref
Modified hydrothermal Solid-state reaction	$\text{Li}_{1.2}\text{Mn}_{0.54}\text{Ni}_{0.13}\text{Co}_{0.13}\text{O}_2$	300 mAh/g	235 mAh/g	78.33%	[10]
	$\text{Li}_{1.2}\text{Ni}_{0.18}\text{Mn}_{0.58}\text{Co}_{0.04}\text{O}_2$	318 mAh/g	235 mAh/g	73.89%	[14]
	$\text{Li}_{1.2}\text{Ni}_{1/6}\text{Co}_{1/6}\text{Mn}_{4/6}\text{O}_{2.35}$	324 mAh/g	250 mAh/g	77.16%	[15]
Co-precipitation					
Sol-gel	$\text{Li}_{1.2}\text{Ni}_{0.15}\text{Mn}_{0.55}\text{Co}_{0.1}\text{O}_2$	339 mAh/g	236 mAh/g	69.61%	[22]
Sol-gel	$\text{Li}_{1.2}\text{Mn}_{0.54}\text{Ni}_{0.13}\text{Co}_{0.13}\text{O}_2$	338 mAh/g	262.5 mAh/g	77.66%	This work

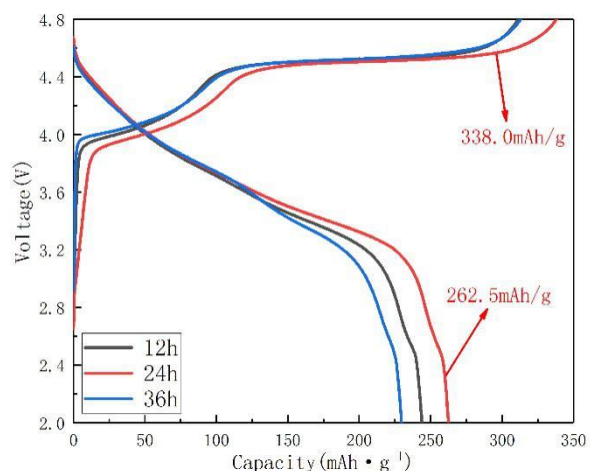


Figure 5. The first charge and discharge curve of the sample.

To compare the electrochemical redox reactions of the three samples, cyclic voltammetry (CV) measurements were performed. As shown in Fig. 6, two distinct platforms emerged during the first charging process, corresponding to the platforms of the two charging curves in Fig. 5. Two peaks of 3.9 V and 4.6 V appeared on the first CV scan curve, which may be due to the oxidation of Ni^{2+} and Co^{3+} and the removal of Li^+ ions in the structure, accompanied by the release of oxygen. Two distinct reduction peaks of approximately 3.7 V and 3.3 V can be clearly observed in the reverse scan, which can be attributed to the reduction of Ni^{3+} and Mn^{4+} [7,26].

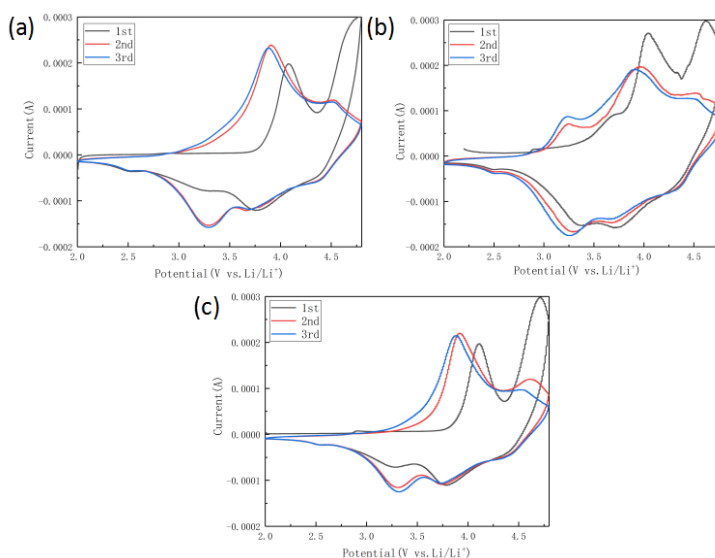


Figure 6. Cyclic voltammetry (CV) curves at different drying times. (a) 12 h, (b) 24 h, and (c) 36 h.

The oxidation peak of 4.5 V is obvious and sharp, and the main reason for this is that Li^+ continuously escaped with the release of oxygen and finally came out of the Li_2MnO_3 component of the material in the form of Li_2O . In the next cycle, the oxidation peak disappeared, indicating that the

reaction is irreversible [27]. The samples dried in the first cycle for 24 h had partial changes with drying for 12 h and 36 h. First, there is a significant difference in the relative proportions of these two oxidation peaks at 3.9 V and 4.6 V. The ratio of the oxidation peak current $I_{(4.6V)}/I_{(3.9V)}$ is defined as R, and the lower $I_{(4.6V)}/I_{(3.9V)}$ value represents a stable structure. It is clear that the sample dried for 24 h had the most stable structure [28].

Figure 7 is a graph showing the rate performance of $Li_{1.2}Mn_{0.54}Ni_{0.13}Co_{0.13}O_2$ after drying for 12 h, 24 h and 36 h. The electrochemical test voltage was adjusted from 2.0 V to 4.8 V at different current densities of 0.1 C, 0.2 C, 0.5 C, 1 C, 2 C, 5 C and back to 0.1 C (1 C=200 mAh/g). A charge and discharge test was performed. As seen from the figure, the sample with a drying time of 24 h had a better rate performance. It can be seen from the figure that the discharge capacity of all the samples decreased as the charge and discharge current increased. At the same charge and discharge current, especially at high currents (1.0 C and 2.0 C), the sample having a drying time of 24 hours had a higher discharge specific capacity.

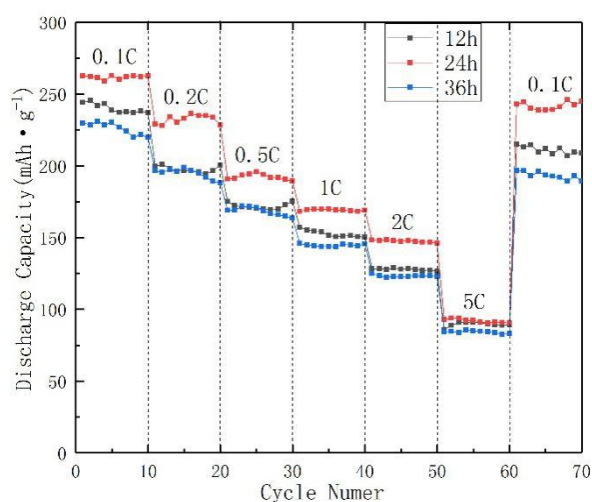


Figure 7. The rate capability of samples synthesized with different drying times.

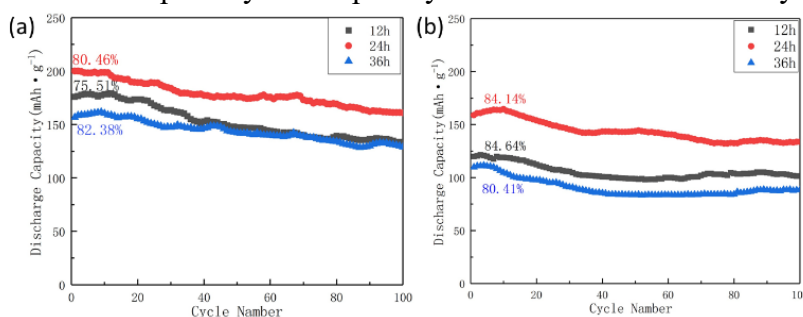


Figure 8. Cycle performance of the different drying times materials. (a) 0.5 C and (b) 2 C.

Fig. 8 is a graph comparing the discharge specific capacity of a synthetic material at a voltage range of 2-4.8 V and a current density of 0.5 C and 2 C for 100 cycles at different drying times. The discharge specific capacity of the sample gradually increased during the first three cycles due to the extension of the 3.5 V high voltage, indicating that it took several cycles to fully activate the Li_2MnO_3 phase. [29] With the increase in the number of cycles, the discharge capacity of all materials decreased,

and the discharge specific capacity was the highest after drying for 24 hours after 100 weeks of cycling, reaching 161.0 mAh/g and 133.7 mAh/g at 0.5 C and 2 C, respectively. For the first discharge capacity, the capacity retention rates were 80.46% and 84.14% at 0.5 C and 2 C, respectively.

To better observe the effect of drying time on the electrochemical performance of the material, all samples were tested for AC impedance in the uncharged cycle, as shown in Fig. 9. The impedance spectra of all samples consisted of a semicircle in the mid-high frequency region and a diagonal line in the low-frequency region. The semicircle corresponds to the charge transfer resistance (R_{ct}) between the material and the electrolyte interface, while the oblique line is related to the Warburg impedance (W_s), which is related to the transfer of Li^+ in the active material [15,30]. The sample dried for 24 h had the lowest charge transfer impedance, which indicates that lithium ions can be quickly deintercalated through the material interface, consistent with the results in the rate performance test.

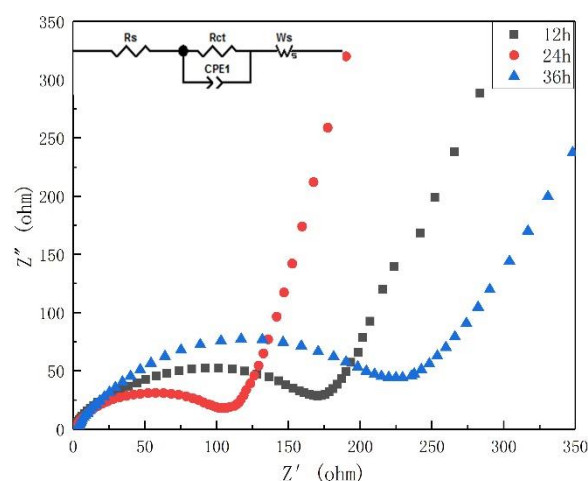


Figure 9. AC impedance of samples synthesized with different drying times.

4. CONCLUSIONS

In this work, a material was prepared by a sol-gel method by controlling different drying times. XRD showed that the drying time had a significant effect on the layered structure of the material and the degree of cation mixing. By testing CV, it was found that the material structure for drying for 24 hours was the most stable. The results of the electrochemical tests show that the $\text{Li}_{1.2}\text{Mn}_{0.54}\text{Ni}_{0.13}\text{Co}_{0.13}\text{O}_2$ material had the best electrochemical performance when the drying time was 24 h. The first discharge specific capacity at 0.1 C is as high as 262.5 mAh/g, and its first efficiency was 77.66%. The discharge-specific capacity was maintained at 161.0 mAh/g and 133.7 mAh/g after cycling for 100 cycles at high current (0.5 C and 2.0 C). Its capacity retention rate reached 80.46% and 84.14% at 0.5 C and 2.0 C, respectively. We hope that these studies will play an important role in the further development of lithium-rich manganese-based materials.

ACKNOWLEDGEMENTS

This work was financially supported by the National Natural Science Foundation of China (Grant

No.11264023) and the Natural Science Foundation of Gansu Province, China (Grant No. 1210ZTC035)

References

1. J.-L. Shi, D.-D. Xiao, X.-D. Zhang, Y.-X. Yin, Y.-G. Guo, L. Gu and L.-J. Wan, *Nano Res.*, 10 (2017) 4201.
2. Y. Zhang, Y. Li, X. Niu, D. Wang, D. Zhou, X. Wang, C. Gu and J. Tu, *J. Mater. Chem. A*, 3 (2015) 14291.
3. W. X. Su, W. J. Feng, Y. Cao, L. J. Cheng, M. M. Li, C. K. Song, *J. Electrochem. Sci.*, 13 (2018) 6005.
4. M. C. Kim, K.-W. Nam, E. Hu, X.-Q. Yang, H. Kim, K. Kang, V. Aravindan, W.-S. Kim and Y.-S. Lee, *ChemSusChem*, 7 (2014) 829.
5. X. Hou, Y. Huang, S. Ma, X. Zou, S. Hu and Y. Wu, *Mater. Res. Bull.*, 63 (2015) 256.
6. T.-F. Yi, W. Tao, B. Chen, Y.-R. Zhu, S.-Y. Yang and Y. Xie, *Electrochimica Acta*, 188 (2016) 686.
7. Y. Liu, D. Ning, L. Zheng, Q. Zhang, L. Gu, R. Gao, J. Zhang, A. Franz, G. Schumacher and X. Liu, *J. Power Sources*, 375 (2018) 1.
8. L. Li, M. Xu, Z. Chen, X. Zhou, Q. Zhang, H. Zhu, C. Wu and K. Zhang, *Electrochimica Acta*, 174 (2015) 446.
9. S. J. Shi, J. P. Tu, Y. Y. Tang, X. Y. Liu, Y. Q. Zhang, X. L. Wang and C. D. Gu, *Electrochimica Acta*, 88 (2013) 671.
10. L. Zhang, K. Jin, L. Wang, Y. Zhang, X. Li and Y. Song, *J. Alloys Compd.*, 638 (2015) 298.
11. Y. Bai, Y. Li, C. Wu, J. Lu, H. Li, Z. Liu, Y. Zhong, S. Chen, C. Zhang, K. Amine and F. Wu, *Energy Technol.*, 3 (2015) 843.
12. H.-W. Lee, P. Muralidharan, R. Ruffo, C. M. Mari, Y. Cui and D. K. Kim, *Nano Lett.*, 10 (2010) 3852.
13. L. Yu, W. Qiu, F. Lian, J. Huang and X. Kang, *J. Alloys Compd.*, 471 (2009) 317.
14. J. Wang, B. Qiu, H. Cao, Y. Xia and Z. Liu, *J. Power Sources*, 218 (2012) 128.
15. J. Wang, G. Yuan, M. Zhang, B. Qiu, Y. Xia and Z. Liu, *Electrochimica Acta*, 66 (2012) 61.
16. A. Tiwari, V. Singh and T. C. Nagaiah, *J. Mater. Chem. A*, 6 (2018) 2681.
17. H. Xu, S. Deng and G. Chen, *J. Mater. Chem. A*, 2 (2014) 15015.
18. Y. Xiang, Z. Sun, J. Li, X. Wu, Z. Liu, L. Xiong, Z. He, B. Long, C. Yang and Z. Yin, *Ceram. Int.*, 43 (2017) 2320.
19. J. Li, R. Klöpsch, M. C. Stan, S. Nowak, M. Kunze, M. Winter and S. Passerini, *J. Power Sources*, 196 (2011) 4821.
20. L. F. Jiao, M. Zhang, H. T. Yuan, M. Zhao, J. Guo, W. Wang, X. D. Zhou and Y. M. Wang, *J. Power Sources*, 167 (2007) 178.
21. K. M. Shaju, G. V. Subba Rao and B. V. R. Chowdari, *Electrochimica Acta*, 48 (2002) 145.
22. T. Tang and H.-L. Zhang, *Electrochimica Acta*, 191 (2016) 263.
23. Y. Cao, W. J. Feng, W. X. Su, *J. Electrochem. Sci.*, 13 (2018) 8022.
24. J.-Z. Kong, C.-L. Wang, X. Qian, G.-A. Tai, A.-D. Li, D. Wu, H. Li, F. Zhou, C. Yu, Y. Sun, D. Jia and W.-P. Tang, *Electrochimica Acta*, 174 (2015) 542.
25. J. Zheng, M. Gu, A. Genc, J. Xiao, P. Xu, X. Chen, Z. Zhu, W. Zhao, L. Pullan, C. Wang and J.-G. Zhang, *Nano Lett.*, 14 (2014) 2628.
26. J.-H. Kim, C. W. Park, Y.-K. Sun, *Solid State Ion.*, 164 (2003) 43.
27. C. S. Johnson, N. Li, C. Lefief, J. T. Vaughey and M. M. Thackeray, *Chem. Mater.*, 20 (2008) 6095.
28. Y. X. Wang, K. H. Shang, W. He, X. P. Ai, Y. L. Cao and H. X. Yang, *ACS Appl. Mater. Interfaces*,

7 (2015) 13014.

29. X.-Y. Liu, J.-L. Liu, T. Huang, A.-S. Yu, *Electrochimica Acta*, 109 (2013) 52.

30. H. Liu, C. Chen, C. Du, X. He, G. Yin, B. Song, P. Zuo, X. Cheng, Y. Ma and Y. Gao, *J. Mater. Chem. A*, 3 (2015) 2634.

© 2019 The Authors. Published by ESG (www.electrochemsci.org). This article is an open access article distributed under the terms and conditions of the Creative Commons Attribution license (<http://creativecommons.org/licenses/by/4.0/>).